ADVANCING EARTH AND SPACE SCIENCES

Geophysical Research Letters

RESEARCH LETTER
10.1029/2026GL122537

Corundum Discovered by SuperCam and the Perseverance Rover at Jezero Crater, Mars

A. M. Ollila[1], O. Beyssac[2], A. Fau[3], O. Forni[3], E. Clavé[4,5], P. Beck[6], C. C. Bedford[7], V. Payre[8], E. Dehouck[4], S. A. Connell[1,7], J. A. Manrique[9], P. Pilleri[3], O. Gasnault[3], G. M. Martinez[10], A. Udry[11], S. Bernard[2], P. Gasda[1], T. Acosta-Maeda[12], R. B. Anderson[13], T. S. J. Gabriel[14], F. Calef[15], J. F. Bell III[16], J. Maki[17], S. Schröder[5], C. Quantin-Nataf[4], J. R. Johnson[17], B. Chide[3], K. Rammelkamp[5], F. Poulet[18], C. Royer[18], M. Rock[1], N. L. Lanza[1], S. K. Sharma[12], G. Lopez-Reyes[9], T. Fouchet[19], J. Comellas[1,12], A. Zastrow[1], E. Cloutis[20], R. C. Wiens[7], A. Cousin[3], S. Maurice[3], S. Clegg[1], P. Bernardi[19], and T. Nelson[1]

[1]Los Alamos National Laboratory, Los Alamos, NM, USA, [2]Institut de Minéralogie, de Physique des Matériaux et de Cosmochimie, CNRS UMR 7590, Muséum National d'Histoire Naturelle, Sorbonne Université, Paris, France, [3]Institut de Recherche en Astrophysique et Planetologie (IRAP), Université de Toulouse, UPS, CNRS, Toulouse, France, [4]Université de Lyon, UCBL, ENSL, UJM, CNRS, LGL-TPE, Villeurbanne, France, [5]DLR - Institute of Space Research, Berlin, Germany, [6]Institut de Planétologie et d'Astrophysique de Grenoble, Université Grenoble Alpes, Grenoble, France, [7]Purdue University, West Lafayette, IN, USA, [8]School of Earth, Environment, and Sustainability, University of Iowa, Iowa City, IA, USA, [9]ERICA Research Group & LADIS, Universidad de Valladolid, Valladolid, Spain, [10]CSIC-INTA - Centro de Astrobiología (CAB), Torrejon de Ardoz, Spain, [11]Department of Geosciences, University of Nevada Las Vegas, Las Vegas, NV, USA, [12]University of Hawaii, Manoa, HI, USA, [13]Planetary Science Institute, Tucson, AZ, USA, [14]U.S. Geological Survey Astrogeology Science Center, Flagstaff, AZ, USA, [15]Jet Propulsion Laboratory/Caltech, Pasadena, CA, USA, [16]School of Earth and Space Exploration, Arizona State University, Tempe, AZ, USA, [17]Johns Hopkins University Applied Physics Laboratory, Laurel, MD, USA, [18]Institut d'Astrophysique Spatiale, Université Paris-Saclay, Orsay, France, [19]LIRA, Observatoire de Paris, Université PSL, CNRS, Sorbonne Université, Université Paris Cité, Meudon, France, [20]University of Winnipeg, Winnipeg, MB, Canada

Key Points:

- For the first time, corundum (α-Al_2O_3) has been identified on Mars. It is found within plagioclase-rich pebbles on the Jezero crater rim
- Corundum was identified by the presence of distinctive Cr^{3+} spectral peaks using time-resolved luminescence spectroscopy
- Corundum broadens the mineral types found on Mars to include magmatic or metamorphic minerals formed in high Al/low Si environments

Supporting Information:

Supporting Information may be found in the online version of this article.

Correspondence to:

A. M. Ollila,
amo@lanl.gov

Citation:

Ollila, A. M., Beyssac, O., Fau, A., Forni, O., Clavé, E., Beck, P., et al. (2026). Corundum discovered by SuperCam and the Perseverance rover at Jezero crater, Mars. *Geophysical Research Letters*, *53*, e2026GL122537. https://doi.org/10.1029/2026GL122537

Received 8 JUN 2026
Accepted 23 JUL 2026

Author Contributions:

Conceptualization: A. M. Ollila, O. Beyssac, E. Clavé, C. C. Bedford, V. Payre, A. Udry, P. Gasda, N. L. Lanza, R. C. Wiens, A. Cousin, S. Maurice, T. Nelson
Data curation: A. M. Ollila, E. Clavé, P. Pilleri, J. F. Bell III, J. Maki, G. Lopez-Reyes, R. C. Wiens
Formal analysis: A. M. Ollila, O. Beyssac, A. Fau, O. Forni, E. Clavé, P. Beck, C. C. Bedford, V. Payre, E. Dehouck, S. A. Connell, J. A. Manrique, P. Pilleri, G. M. Martinez, A. Udry,

Abstract

Mars is primarily composed of mafic mineral assemblages and their alteration products, but small, scattered rocks strewn across the landscape offer clues to greater petrological diversity. While traversing the Jezero crater rim, the Perseverance rover encountered several plagioclase-rich light-toned float rocks. SuperCam identified the distinctive signature of corundum (α-Al_2O_3) in these rocks using time-resolved luminescence spectroscopy. Two strong peaks (692.7 and 694.1 nm) with millisecond lifetimes, and additional supporting lines, are consistent with Cr^{3+} substitution for Al^{3+} in corundum. Corundum forms in Al-rich, Si-depleted environments through magmatic or metamorphic processes. Given the rocks' small size, association with plagioclase, and location on the crater rim, we interpret the most plausible formation scenario to be impact induced metamorphism at the interface of a felsic and a mafic/ultramafic member with the likely action of fluids at some stage, although other possibilities are not excluded.

Plain Language Summary

Minerals provide clues to the type of geologic environments in which they form. The primary types of minerals that have been identified on Mars indicate a history dominated by volcanism followed by interaction with water. However, other minerals that tell a different story are sometimes found. Here we present results from the SuperCam instrument on the Perseverance rover in which the mineral corundum (α-Al_2O_3) has been identified using a technique called time-resolved luminescence spectroscopy. Corundum has a unique light-emitting (luminescence) feature based on two well-known peaks as well as the time it takes for this light to fade after being excited by a laser, which is referred to as the lifetime. Corundum forms in specific environments that are enriched in aluminum and depleted in silicon and have been subjected to high temperature and pressure. Such places include deep subsurface magmas or shallower locations that have been exposed to high temperature through tectonic processes or meteorite impacts. Given their small sizes, association with the mineral plagioclase, and locations on the heavily impacted crater rim, we propose that these corundum minerals formed through impact processes.

S. Bernard, P. Gasda, T. Acosta-Maeda, R. B. Anderson, T. S. J. Gabriel, S. Schröder, B. Chide, K. Rammelkamp, M. Rock
Funding acquisition: O. Gasnault, R. C. Wiens, A. Cousin, S. Maurice
Investigation: A. M. Ollila, O. Beyssac, A. Fau, O. Forni, P. Beck, E. Dehouck, O. Gasnault, S. Bernard, R. B. Anderson, T. S. J. Gabriel, J. F. Bell III, J. Maki, C. Quantin-Nataf, J. R. Johnson, B. Chide, K. Rammelkamp, F. Poulet, C. Royer, N. L. Lanza, S. K. Sharma, G. Lopez-Reyes, T. Fouchet, J. Comellas, A. Zastrow, E. Cloutis, R. C. Wiens, A. Cousin, S. Maurice, S. Clegg, P. Bernardi, T. Nelson
Methodology: A. M. Ollila, O. Beyssac, A. Fau, O. Forni, E. Clavé, C. C. Bedford, V. Payre, E. Dehouck, S. A. Connell, J. A. Manrique, P. Pilleri, O. Gasnault, G. M. Martinez, A. Udry, S. Bernard, T. Acosta-Maeda, R. B. Anderson, T. S. J. Gabriel, F. Calef, J. F. Bell III, J. Maki, S. Schröder, C. Quantin-Nataf, J. R. Johnson, B. Chide, K. Rammelkamp, F. Poulet, C. Royer, M. Rock, S. K. Sharma, G. Lopez-Reyes, T. Fouchet, J. Comellas, A. Zastrow, E. Cloutis, R. C. Wiens, A. Cousin, S. Maurice, S. Clegg, P. Bernardi, T. Nelson
Project administration: O. Gasnault, R. C. Wiens, A. Cousin, S. Maurice, S. Clegg, P. Bernardi
Software: F. Calef
Supervision: O. Gasnault, R. C. Wiens, A. Cousin, S. Maurice
Validation: A. M. Ollila, O. Beyssac, A. Fau, T. Acosta-Maeda, T. Nelson
Visualization: F. Calef
Writing – original draft: A. M. Ollila, O. Beyssac, A. Fau, O. Forni, E. Clavé, P. Beck, C. C. Bedford, V. Payre, E. Dehouck, S. A. Connell, J. A. Manrique, O. Gasnault, G. M. Martinez, A. Udry, S. Bernard, P. Gasda, S. Schröder, C. Quantin-Nataf, J. R. Johnson, B. Chide, K. Rammelkamp, F. Poulet, S. K. Sharma, T. Fouchet, A. Zastrow, E. Cloutis, R. C. Wiens, A. Cousin
Writing – review & editing: A. M. Ollila, O. Beyssac, A. Fau, O. Forni, E. Clavé, P. Beck, C. C. Bedford, V. Payre, E. Dehouck, S. A. Connell, J. A. Manrique, O. Gasnault, G. M. Martinez, A. Udry, S. Bernard, P. Gasda, S. Schröder, C. Quantin-Nataf, J. R. Johnson, B. Chide, K. Rammelkamp, F. Poulet, S. K. Sharma, T. Fouchet, A. Zastrow, E. Cloutis, R. C. Wiens, A. Cousin

1. Introduction

Corundum (α-Al_2O_3) is a mineral that forms in restricted Al-rich and Si-poor magmatic or metamorphic settings. Pure corundum is colorless; its color is controlled primarily by trace element substituents: Cr^{3+} produces red/pink colors (i.e., ruby) and Fe^{2+}, Fe^{3+}, Ti^{4+}, and V^{3+} produce various other colors (i.e., sapphire, Dubinsky et al., 2020). Corundum occurs in many geological environments on Earth (Giuliani et al., 2020; Simonet et al., 2008) and occurs rarely in extraterrestrial materials, for example, meteorites and lunar materials (Kleinmann, 1971; Li et al., 2020; Nittler et al., 1997; Zhang et al., 2021). Corundum has not previously been identified on Mars from orbit, in situ, or in meteorites.

The Perseverance rover landed on the floor of Jezero crater, Mars on 18 February 2021 to study an ancient lake-associated deltaic fan system and local igneous units and to cache samples for future return to Earth (Farley et al., 2020; Simon et al., 2023). Perseverance has a comprehensive payload designed to analyze the rocks and soils of Jezero (Farley et al., 2020), including the SuperCam instrument (Maurice et al., 2021; Wiens et al., 2021). SuperCam has the capability to determine both chemical composition and mineralogy using co-located spectroscopy techniques. Here, we use SuperCam's time-resolved luminescence (TRL) spectroscopy to identify corundum on Mars for the first time. To do this, we use the extreme sensitivity and reliability of luminescence to detect trace elements in minerals, here Cr^{3+} in corundum (Gaft et al., 2005, 2015). This observation was done on light-toned float (LTF) rocks found in the Jezero crater rim. We first discuss the detection of corundum as well as the petrology of these rocks. Then we analyze the possible implications for the mineralogical diversity and the geological history of Mars by reviewing formation processes of corundum.

2. Geological Context

After exploring the Jezero crater floor, the sedimentary fan, the margin unit, and Neretva Vallis, Perseverance began the exploration of the crater rim on sol 1252. Preliminary investigations of the crater rim revealed the presence of rocks with distinct petrology including phyllosilicate-rich altered bedrocks, impact breccias, pyroxenites, and plagioclase-rich rocks (Quantin-Nataf et al., 2025; Udry et al., 2025). Additional mineralogical diversity has been found in Jezero in various float rocks of unknown provenance, including hydrated silica and quartz (Beck et al., 2025) and Al-rich minerals like kaolinite/halloysite and spinel (Royer et al., 2024). While none of these lithologies can be directly tied to the corundum-bearing LTF rocks studied here, they do provide evidence for crustal diversity, fluid-rock interactions, and hydrothermal processes acting at various depths and through various host rocks up to the surface.

The corundum-bearing LTF rocks were discovered as small fragments of plagioclase-rich rocks on the crater rim (Figure 1, Figures S1–S3 in Supporting Information S1) and were not observed on the other units (although we cannot exclude their presence). Table S1 in Supporting Information S1 lists the plagioclase-bearing rocks investigated here, which can be divided into two groups. The first group includes the three targets on which Cr-bearing corundum was detected by TRL (Hampden_River, Coffee_Cove, and Smiths_Harbor); the second group includes other LTF with similar bulk composition, but which apparently lack Cr-bearing corundum (either absent or not detected; Sams_River, Leading_Tickles, and Fisherbekkene). Notably, the first two corundum-bearing targets, Hampden_River and Coffee_Cove, were found only a few meters apart (at the Sallys_Cove outcrop) while the third one, Smiths_Harbor, was found about 100 m to the south (Figure S1 in Supporting Information S1). Targets from the second group were found in the same area as these targets. For reference, other plagioclase-bearing rocks from elsewhere (Witch Hazel Hill, Eagle Cliff, and Maaz) are included in Tables S1 and S2 and Figure S1 in Supporting Information S1. This paper covers targets analyzed through sol 1554 (2 July 2025).

3. Methods

The SuperCam instrument uses multiple analytical methods to determine the chemistry and mineralogy of rocks and soils at meters distances from the rover (Maurice et al., 2021; Wiens et al., 2021). Chemical compositions are obtained primarily from laser-induced breakdown spectroscopy (LIBS); TRL can provide information on the presence of trace elements. Mineralogy can be determined by time-resolved Raman (TRR) and visible-near infrared (VISIR) spectroscopy. A Remote Micro-Imager (RMI) takes high-resolution images, which provide context for the analysis locations. The analytical and imaging instruments are co-boresighted, so they obtain data from the same general areas, but the footprints vary by technique and thus the results may not be for completely

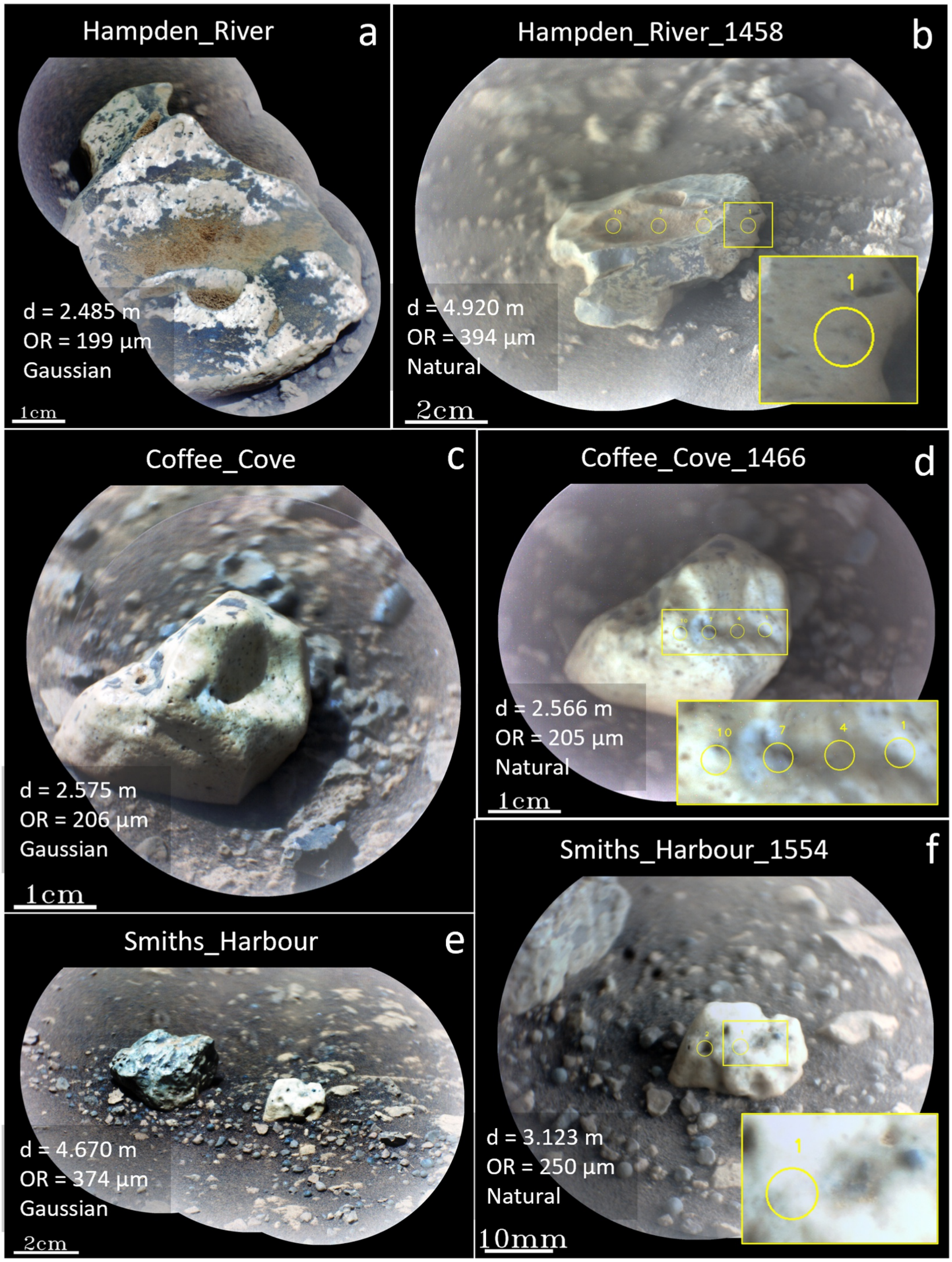

Figure 1. SuperCam RMIs of the targets with luminescence signatures attributed to Cr^{3+} in corundum. Distance to target (d), optical resolution (OR), and processing (Gaussian stretch or Natural) are given on each image. Locations and FOVs where luminescence spectra were obtained are marked with yellow circles. Insets are shown for the points exhibiting Cr^{3+}luminescence. The light-toned portion of each of these rocks has a plagioclase composition. (a) Hampden_River (sol 1453). (b) Hampden_River (sol 1458), ~5 m from the previous rover location. (c) Coffee_Cove (sol 1465). (d) Coffee_Cove (sol 1466). (e) Smiths_Harbor (sol 1551). (f) Smiths_Harbor (sol 1554).

identical materials. SuperCam has various modes for collecting data to maximize efficiency while conceding to limitations in activities due to rover constraints such as available power, time, and data volume. These operational modes are described in more detail in Text S1 in Supporting Information S1.

SuperCam's high-resolution color RMI images provide textures and contexts from sub-mm (mineral grains and LIBS ablation pits) to meter scales (i.e., geomorphic structures); these are available as natural red-blue-green images and with a Gaussian stretch to enhance contrast. By design, the RMI achieves an effective image resolution better than 80 microradians, which corresponds to ≤0.24 mm on a target at 3 m distance (Maurice et al., 2021). These images are placed in context by those of Perseverance's NavCam (Maki et al., 2020) and MastCam-Z (Bell et al., 2021) imaging systems.

SuperCam LIBS uses a pulsed 1064 nm laser to ablate a target, forming a plasma of excited species. Light emitted from the plasma is collected by spectrometers, covering the spectral ranges from 245–340, 385–465, and 535–853 nm. The spectra of emitted light are categorized to specific elemental (and molecular) ionic transitions, and the strengths of those emissions are converted to elemental abundances in the target using multivariate techniques (Anderson et al., 2022). As discussed by Anderson et al. (2022), the calibration models accuracies in root mean square error of prediction in wt. %, are: CaO (1.3), FeO (3.1), Na_2O (0.5), K_2O (0.6), MgO (1.1), SiO_2 (6.1), Al_2O_3 (1.8), and TiO_2 (0.3). Oxide totals often do not sum to 100% due to accuracy errors and non-quantified components (see Text S1 in Supporting Information S1). Compositions are used to test for stoichiometric mineralogy following criteria described in Beyssac et al. (2023, 2026) and Udry et al. (2023). LIBS data have been filtered following the criteria described in Beyssac et al. (2023) and data contaminated by coatings and/or dust were also removed after careful examination of LIBS bulk and single-pulse data as well as inspection of RMI images before and after LIBS analyses. The analytical footprint is ∼100–450 μm (1.5–7 m), depending on the distance.

The SuperCam TRR technique uses a collimated pulsed 532 nm laser (frequency doubled 1,064 nm laser) to probe a target and collects Raman-scattered photons in the range of 140–4,500 cm^{-1} with a wavenumber calibration accuracy of ∼1.0 cm^{-1}. The pulsed laser and time gated detector enable a 100 ns gate width, thereby rejecting the majority of signals from mineral luminescence and sunlight entering the telescope. Instrumental artifact Raman signals observed due to the SuperCam design are detailed in Text S1 in Supporting Information S1 (Clavé et al., 2023; Maurice et al., 2021). The analytical footprint is the same for TRR and TRL and varies with the distance to the target (field of view (FOV) = 0.75 mrad; Wiens et al., 2021). Raman spectra are normally obtained by averaging the signal from 400 laser pulses for each analyzed point.

SuperCam's TRL method uses the same pulsed 532 nm laser as TRR and covers the same spectral range (535–853 nm) and has the same FOV. Mineral luminescence commonly have a long lifetime, so TRL analyses are done at night and use long integration times to improve the signal-to-noise ratio. Luminescence spectra can be collected at multiple time intervals to allow estimation of a luminescence center's lifetime (the time required for emission intensity to decay to $1/e$). Identification of luminescence peak centers, areas, and lifetimes follow the methodology described by Fau et al. (2022).

A description of laboratory instruments used to collect TRL reference spectra and VISIR methods are provided in Text S2 and S3 in Supporting Information S1, respectively.

4. Results

4.1. Textural Analysis

We first examine imaging data to provide visual and textural context for three LTF where we identified the presence of corundum with TRL: Hampden_River, Coffee_Cove, and Smiths_Harbor (Figure 1). Unstretched color images with LIBS, VISIR, and Raman/TRL FOV are shown in Figure S4 in Supporting Information S1. Other plagioclase-bearing float rocks are shown in Figure S5 in Supporting Information S1. These LTF are centimeter-sized fragments of light-toned rocks which appear homogeneous at the spatial resolution of the RMI. From these images, one cannot detect discrete grains of corundum nor determine the grain size(s) of the plagioclase. Most of these rocks show darker areas which are interpreted as patches of coating adhering to the rock surface (Garczynski et al., 2025). Some dust is also visible locally on the rocks' surfaces. These dark and/or dusty patches are not discussed further, as they are not representative of the bulk lithology of the rocks. Some of the plagioclase-rich rocks that did not display luminescence attributed to Cr^{3+} in corundum (e.g., Fisherbekkene or Leading_Tickles), show small darker areas in the light-toned matrix; these are interpreted as grains of dark-toned, currently unidentified minerals and not surficial coatings.

4.2. Chemistry and Mineral Composition From LIBS

For geochemical context for the plagioclase-rich LTF rocks, LIBS compositional data are shown in Figure 2, Figure S6, Table S2–S3 in Supporting Information S1. Most LIBS analyses for Hampden_River were consistent with compositions of dust or coatings and were rejected for this study. In the Si + Al - Ca + Na + K - Fe + Mg ternary diagram (Figure 2a), all LIBS compositions cluster toward that of the on-board andesine calibration target (Cousin et al., 2022), suggesting that the rocks consist mostly of plagioclase. The composition of Coffee_Cove corresponds to stoichiometric plagioclase with the composition $An_{35\text{-}48}Ab_{50\text{-}60}Or_{1\text{-}7}$, while most other targets also have a composition close to stoichiometric plagioclase (Figure 2b, Table S3 in Supporting Information S1). Only four additional stoichiometric plagioclase analysis points were identified in the other LTF (Sams_River, Fisherbekkene, and Smiths_Harbor, Table S2 in Supporting Information S1) with composition $An_{35\text{-}42}Ab_{51\text{-}55}Or_{7\text{-}11}$. Notably, no significant excess of Al_2O_3 relative to stoichiometric plagioclase was detected in any target. Minor FeO and MgO are detected and may be due to the presence of a ferromagnesian mineral, a phyllosilicate based on VISIR data (see Section 4.3). No excess light elements (C, S, H) or trace elements (specifically Cr) were detected, except Sr. Point 5 of Fisherbekkene is close to the high-Ca pyroxene standard but was inconsistent with stoichiometric pyroxene. In the RMI, it corresponds to a dark area below some dust.

Independent Component Analysis (Forni et al., 2013) was performed using stoichiometric plagioclase spectra from Mars and laboratory plagioclase spectra (Figure S7, Table S4 in Supporting Information S1) to confirm the Mars plagioclase are more similar to intermediate composition plagioclase, that is, andesine, than to the end-members anorthite or albite. This composition of plagioclase has been observed in other units of the Jezero region (Figure S6, Table S2 in Supporting Information S1).

4.3. Mineralogy From Raman and VISIR Spectroscopy

One dedicated Raman analysis was acquired from Coffee_Cove, which showed a single peak at $\sim$508 cm^{-1} with a FWHM of 12–17 cm^{-1}. These parameters are consistent with those of the strongest Raman peak from crystalline plagioclase at $\sim$506–508 cm^{-1} which has a FWHM of 7–20 cm^{-1} (Figure 2c, Bersani et al., 2018). The positions of this peak shift slightly with the plagioclase composition (Bersani et al., 2018). No other Raman features, including those of hydration, were detected in any spectrum.

VISIR data show the possible presence of an Al-rich clay mineral in Hampden_River while the spectra of Coffee_Cove and Smiths_Harbor are more consistent with a Mg-rich clay like saponite (Text S3, Figure S8 in Supporting Information S1). Note that neither plagioclase nor corundum have diagnostic absorption bands in the wavelength ranges covered by the SuperCam VISIR spectrometers (Figure S8 in Supporting Information S1), precluding their detection by this technique (Text S3 in Supporting Information S1).

4.4. Detection of Cr^{3+} in Corundum by Time-Resolved Luminescence

The luminescence spectra from Hampden_River, Coffee_Cove, and Smiths_Harbor show prominent peaks at 692.7 and 694.1 nm (Figure 3a and Figure S9 in Supporting Information S1). Based on their positions and relative intensities, these peaks are interpreted to be the R2 and R1 transitions produced by the substitution of Cr^{3+} for Al^{3+} in corundum (Gaft et al., 2015; Guguschev et al., 2010), which have been extensively studied for decades in solid state physics (Syassen, 2008). For comparison, Figure 3a shows luminescence spectra of Hampden_River_1458 and Coffee_Cove_1466 compared to laboratory spectra of natural ruby, ruby in amphibolite, and diaspore, a hydrated low-temperature Al-oxy-hydroxide, AlO(OH), a mineral with similar R-line peak positions. Photographs of these samples are in Figure S10 in Supporting Information S1. Additional laboratory spectra, including that of sapphire are shown in Figure S11 in Supporting Information S1. The sapphire spectra are consistent with the Mars data as well due to the presence of Cr^{3+}, in addition to the Fe^{2+}-Ti^{4+} charge-transfer absorption that creates the blue color commonly found in sapphire. The luminescence peak positions eliminate diaspore as a potential candidate. Other minerals have been excluded based on their published luminescence spectra, for example, plagioclase and other common martian minerals (Table S5 in Supporting Information S1) or minerals with known Cr^{3+} peaks in this region, for example, kyanite, spinel, and emerald (Table S6 in Supporting Information S1) (Gaft et al., 2015; Galili et al., 2023; Okumura et al., 2006). The downshift of −0.3 nm in peak position of the Mars data compared to laboratory data may be explained by

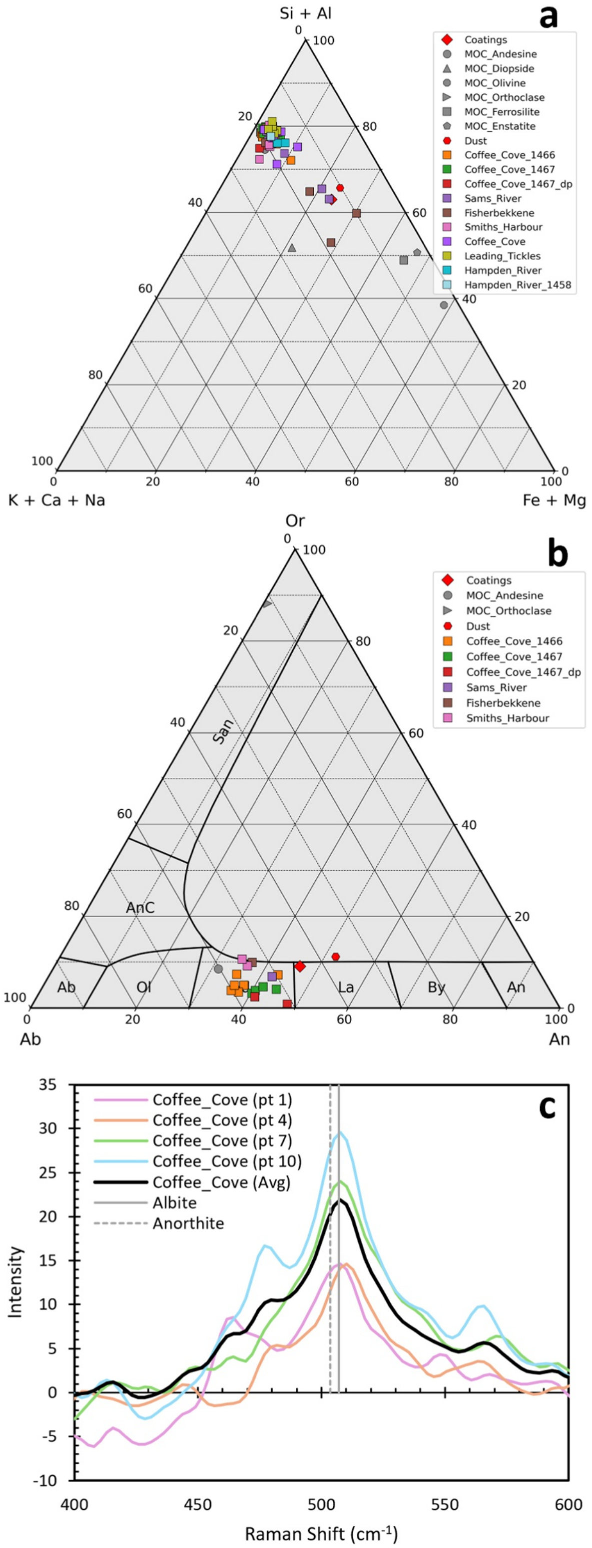

Figure 2.

a combination of factors, but the primary cause is likely that Mars' ambient temperature is significantly cooler compared to the typical laboratory. Using the relationship between peak position and temperature derived by Ragan et al. (1992), these luminescence peak positions are consistent with temperatures between the minimum measured in the area (222 K) by the Mars Environmental Dynamics Analyzer instrument (Rodriguez-Manfredi et al., 2021, Text S4 and Figure S12 in Supporting Information S1), and laboratory room temperature (~300 K), seen in Figure 3a. Pressure (Forman et al., 1972; Kobayashi et al., 2004; Piermarini et al., 1975; Syassen, 2008) and radiation damage (Schuster et al., 2010) may also influence the peak positions. Other trace substituents can also shift luminescence peak positions, as has been documented for the mineral beryl (Moroz et al., 2000; Thompson et al., 2014). However, temperature is likely the strongest contributing factor for the observed peak shifts.

In addition to the R-lines, weaker luminescence N-lines (neighbor lines) and vibronic sidebands can also be detected from samples with strong (saturated) R-lines (Figure 3b). The clearest peaks are at ~699.4, 701.5, 704.7, and 707.3 nm and match those observed in the similarly saturated spectra of terrestrial corundum analyzed with the SuperCam development unit (see Text S2 in Supporting Information S1) as well as those described in Guguschev et al. (2010), Raghavan et al. (2008), and Rothamel et al. (1983).

A broad luminescence feature at longer wavelengths, >720 nm, was observed in spectra from several targets: Hampden_River, Coffee_Cove, Leading_Tickles, and Fisherbekkene. This luminescence can be attributed to Fe^{3+} substituting for Al^{3+} in plagioclase, but it is difficult to determine conclusively due the weakness of the feature and wide wavelength range over which this luminescence can manifest (Gaft et al., 2015).

The final piece of evidence confirming the identification of corundum is the lifetime analysis of luminescence from Smiths_Harbor. Figure 3c shows the spectra (inset) and decay obtained at time delays from 0 (laser active on the target) to 1.5 ms after the laser has ceased firing in 0.5 ms intervals for diaspore, ruby, and ruby in amphibolite compared to Smiths_Harbor. To determine the lifetime of the luminescence, the area under the combined R1 and R2 peaks (Figure S13 in Supporting Information S1) is plotted against the time delay, and the luminescence lifetime is the slope of the line going through the experimental points (Fau et al., 2022). The Smiths_Harbor luminescence has a lifetime between those determined for the two terrestrial corundum samples (Figure 3c). The lifetime for Smiths_Harbor is ~3 ms for the combined R-lines, which is consistent with lifetimes determined for terrestrial corundum samples (Gaft et al., 2015; Giuliani et al., 2020). The variations in luminescence lifetimes in corundum reflect both the Cr^{3+} concentration (which can quench the luminescence) and/or the effects of charge transfers to other trace substituents like Ti^{4+}, Ti^{3+}, and Fe^{3+}.

Figure 2. (a) Si + Al−Ca + Na + K−Fe + Mg molar ternary diagram of laser-Induced breakdown spectroscopy (LIBS) compositions for the plagioclase-bearing light-toned float (LTF). Compositions cluster around the composition of the andesine plagioclase LIBS calibration target (MOC_Andesine) measured on Mars. (b) Plagioclase compositions for LIBS plagioclase calibration targets, LTF rocks, and typical dust and rock coatings. The LIBS plagioclase calibration targets and LTF analyses fall in the field of andesine compositions. (c) Raman spectra of Coffee_Cove plotted with markers for albite and anorthite peak positions (Bersani et al., 2018). Intensity is in photons.

10.1029/2026GL122537

5. Discussion

5.1. Corundum-Bearing and Plagioclase Dominated Rocks on Mars

LIBS and Raman data are consistent with these rocks being composed dominantly of plagioclase feldspar, with compositions of $An_{35\text{-}48}Ab_{50\text{-}60}Or_{1\text{-}7}$. Corundum was identified in some of the LTF rocks only from the TRL spectra—there was no evidence of corundum in the LIBS, Raman, or VISIR data. While luminescence spectroscopy is not considered a mineralogical identification technique, in certain cases such as we have here, the Cr^{3+} peaks and their lifetimes can be considered diagnostic of a specific mineralogy (Hainshwang et al., 2024). The TRL detection was possible only because the luminescence is extremely sensitive to parts per million of Cr^{3+} in corundum (Dubinsky et al., 2020). Corundum could, in theory, be detectable by Raman, LIBS, and visible images if its grains were large or abundant enough; the absence of these detections suggests that the corundum grains are small and/or rare. We estimate grain sizes of <200–375 μm based on the RMI optical resolution at the observation distances, ~2.4–5 m (Maurice et al., 2021). From the available data, we cannot rule out that other minor phases are present, like ferromagnesian minerals (amphibole, biotite, and/or pyroxene) and/or accessory phases (zircon or spinel).

5.2. Origin of Corundum

Corundum is a relatively uncommon mineral on Earth and is known from only a few extraterrestrial occurrences. Its formation generally requires bulk compositions enriched in Al and depleted in Si and typically forms at either high temperatures (e.g., in calcium-aluminum inclusions in chondrites, Nittler et al., 1997) or in association with tectonic processes (e.g., Giuliani et al., 2020; Stern et al., 2013). Hence, its detection in martian rocks is surprising.

Mineral assemblages including plagioclase and corundum are found in two broad categories of environments in planetary systems: magmatic and metamorphic (Giuliani et al., 2020; Simonet et al., 2008). On Earth, magmatic versus metamorphic corundum may be distinguished by trace element patterns and/or mineral inclusions, but such a determination is not straightforward (Baldwin et al., 2017; Palke et al., 2018) and cannot be done with our data. In addition, metamorphism often involves metasomatism where fluids facilitate elemental exchange between compositionally distinct rock units, and/or happens at pressure-temperature conditions favorable for partial melting making the distinction even more challenging (Belley et al., 2025). Lastly, a scenario involving impact-related metamorphism must be considered for these rocks found close to shocked impact ejecta deposits uplifted by the Jezero impact. In the following, we present some possible formation processes to test our observations, but this discussion is not intended to be exhaustive.

5.2.1. Magmatic Origin

Corundum is uncommon in igneous rocks like syenites or pyroclastics. Corundum-bearing syenites, igneous rocks rich in alkali feldspar, are rare and typically contain little (or no) plagioclase (J. H. Liu et al., 2022; Rogers, 1911). More commonly, corundum grains, up to centimeters in size, are found as xenocrysts in igneous rocks, ranging from silicic tuffs to basalts to kimberlites (Giuliani et al., 2015; Graham et al., 2008; Kornprobst et al., 1990; Oliveira et al., 2021; Rakotondrazafy et al., 2008). The sources of these xenocrystic corundums are varied, and have been suggested as high-grade crustal metamorphic rocks, or mantle material carried in plumes. The exact formation process of corundum remains challenging to decipher in general: melting of Si-depleted and Al-saturated rocks, or metasomatic processes involving the circulation of deep fluids, or likely the combination of both. Importantly, most corundum-bearing xenoliths or xenocrysts are in rift-related volcanic rocks, implying a connection to plate tectonic processes, which have been suggested for early Mars but not proven. Likewise, magmatic-related corundum on Earth is commonly found as large (>mm) crystals, while our martian finds are much smaller.

5.2.2. Metamorphic/Metasomatic Origin

Metamorphic environments in which corundum can form are varied and can involve high temperatures related to continental collision, lower temperature metasomatism, or hypervelocity impacts. In any case, the presence of corundum imposes relatively high-temperature conditions (>350–400°C) above the diaspore <->

10.1029/2026GL122537

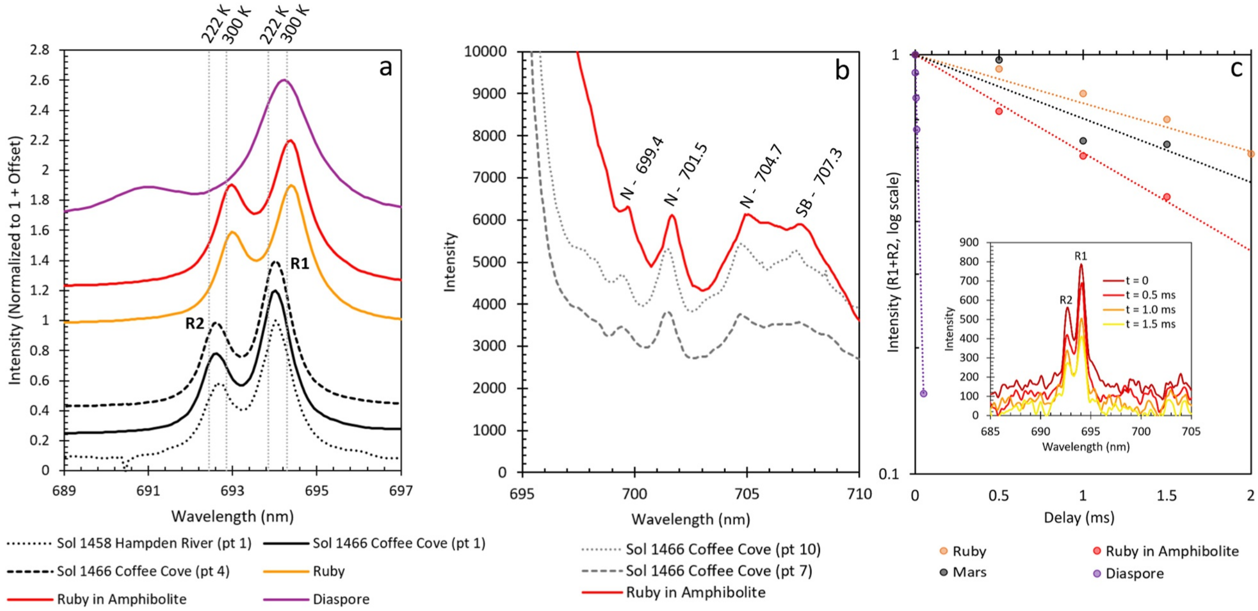

Figure 3. (a) Comparison of luminescence spectral lines (R-lines) from Hampden_River and Coffee_Cove (on Mars with SuperCam TRL) to luminescence spectra (on Earth, with the SuperCam development unit) of two ruby samples and diaspore. Gray vertical lines mark theoretical peak positions of Cr^{3+} luminescence peaks in corundum as functions of temperature (Ragan et al., 1992) (b) Comparison of N-line and sideband spectra from Mars to ruby in amphibolite. (c) Luminescence intensities for Smiths_Harbor compared to laboratory spectra for two ruby samples and diaspore. The main figure shows the logarithms of the luminescence intensities (calculated as areas under the luminescence peaks, inset) versus time. Luminescence lifetimes are calculated from the slopes of these lines. Note that the lifetime of diaspore is very short, and that the luminescence lifetime of Smiths_Harbor is similar to those of the two ruby samples. All intensities are in photons.

corundum + H_2O equilibrium curve (Feenstra & Wunder, 2002) and also specific chemical constraints as the system must be heavily depleted in Si.

Metamorphic corundum is typically found in amphibolite to granulite facies in either mafic-ultramafic rocks or marble (Giuliani et al., 2020) and is often associated with continental collision zones (Stern et al., 2013). The primary types of metamorphic corundum-bearing deposits are aluminous gneiss and granulite, marbles, mafic granulites, and metabauxites (Feenstra & Wunder, 2002; Simonet et al., 2008). Metasomatic deposits include desilicated pegmatites (plumasites), desilicated gneisses, and skarns (e.g., Poulsen et al., 2023; Poulsen et al., 2024; Simonet et al., 2008; Voudouris et al., 2019). Corundum can be closely associated with plagioclase in metamorphic/metasomatic systems, although the plagioclase is often of endmember compositions rather than intermediate as we have here (e.g., Filina et al., 2019; Giuliani et al., 2020; Karmakar et al., 2017; O'Driscoll & Henry, 2025). As there is no conclusive evidence for plate tectonics having occurred on Mars, formation hypotheses requiring such are not favored here. However, metasomatism remains a possibility, as the major requirement of having fluid exchange at the contact between Si-poor and Si- and Al-rich rocks (Simonet et al., 2008) is a feasible scenario in Jezero. Si-poor mafic to ultramafic rocks are present in Jezero (Beyssac et al., 2023; Y. Liu et al., 2022; Wiens et al., 2022). No gneisses or skarns have been as yet identified in the region to serve as the Si-Al-rich component. However, Royer et al. (2024) reported kaolinite-bearing pebbles and cobbles and Beck et al. (2025) identified quartz and opal-bearing float rocks, suggesting hydrothermal activity and a potential source for Al and Si. Due to the martian corundum being associated with plagioclase of andesine composition, a feasible environment could be plumasite-type, formed from desilicated anorthosite (or potentially alkali-feldspar pegmatite). Plumasite deposits on Earth are typically meter-scale in size (Giuliani et al., 2020) and, if formed similarly on Mars, would not readily be observable from orbit. As the rover continues to traverse the crater rim, contact zones and lenses will continue to be analyzed to seek potential source outcrops to determine if this formation hypothesis is likely.

5.2.3. Impact-Related Origins

The surface of Mars retains evidence of numerous impacts, including Jezero crater itself, which is a 45 km impact crater formed during the Noachian on the rim of the 1,900 km diameter Isidis impact structure. Hypervelocity impacts generate shock waves that propagate through the target rocks, brecciating them and variably inducing shock metamorphism (e.g., Bischoff & Stoffler, 1992; Osinski & Pierazzo, 2012). The pressure and temperature regimes achieved by large impacts are comparable to and can exceed those of crustal metamorphic environments (e.g., Osinski & Pierazzo, 2012) in which corundum may form. Corundum was identified in silicate glass in a core from the 85 km diameter Chesapeake Bay impact structure (Horton et al., 2009). It was proposed to have been formed under high-temperature in a Si-undersaturated impact melt. Corundum has also been identified in shock-lithified lunar regolith breccias (Zhang et al., 2021). In these rocks, corundum is found as fine-grained aggregates associated with tissintite (high-vacancy pyroxene structure with the composition essentially equivalent to plagioclase). They propose the corundum formed from intergranular melt and recrystallization due to high pressure and temperature conditions produced by shock metamorphism. A key similarity between impact-formed-corundum and the corundum observed by SuperCam is the small sub-mm grain size. The corundum-bearing LTF rocks are found in the crater rim near what are interpreted to be plagioclase-bearing impact breccia (Charles_Brook and Stuckless_Pond; Figure S1 and S14 in Supporting Information S1; Bedford et al., 2026). While circumstantial, the small grain size, location in the crater rim, and proximity to impact breccias make this a plausible candidate for formation of the corundum.

6. Conclusions

The SuperCam instrument has, for the first time, identified corundum on Mars in the Jezero crater rim in plagioclase-rich float rocks using remote TRL spectroscopy. The TRL technique has proven invaluable to detect apparent sub-mm grains of corundum owing to its extreme sensitivity to the presence of Cr^{3+} as a trace element in corundum. The presence of corundum has important implications for the inventory of geologic processes and environments identified on Mars. The primary questions raised by this discovery are (a) if magmatically derived, are Si-undersaturated Al-rich rocks prevalent on Mars and if so, how did they form (e.g., from crustal assimilation or a mantle source)? (b) Is there evidence of metamorphic processes and if yes, is it similar to terrestrial plate tectonic-related metamorphic activity? As yet there is no evidence for significant plate tectonics having occurred on Mars. Or could it be large impacts inducing pressure-temperature conditions similar to that in tectonic environments? (c) What role did water play in forming the corundum? Is there evidence for hydrothermal/metasomatic processes (either due to impacts or another source), which has astro-biological implications as a potentially habitable environment? While the available evidence is sparse and allows for multiple plausible hypotheses, we favor a formation scenario involving impact-related meta-morphism. Fluid-rock interactions may have also been involved at some stage to trigger the Si depletion and Al enrichment of the protolith rock. To better constrain the formation hypotheses, analysis of a corundum-bearing outcrop would prove useful. If a core sample were obtained from this outcrop and returned to Earth, vastly more analyses could be conducted to conclusively determine how this corundum formed, which would provide a more complete understanding of martian history.

Conflict of Interest

The authors declare no conflicts of interest relevant to this study.

Availability Statement

All mission data are available at the NASA Planetary Data System Geoscience Node at https://pds-geosciences.wustl.edu/missions/mars2020/supercam.htm.

Acknowledgments

The authors thank the SuperCam and Perseverance operations team for their hard work and dedication to the mission. AMO, NLL, PG, AZ, CB, SAC, and RCW were supported by NASA (NNH13ZDA018O). Funding from the Centre National d'Etudes Spatiales (CNES) is acknowledged. Laboratory measurements from IMPMC (Paris) were funded by CNRS INP and Sorbonne Université grants. EAC was supported by the Canadian Space Agency (22EXPCOI4), and the Natural Sciences and Engineering Research Council of Canada (RGPIN-2023-03413 and RTI-2020-00157). GMM acknowledges funding from the Ministry of Science, Innovation and Universities, projects No PID2021-126719OB-C41. JAM and GLR acknowledge funding through the following grants: PID2022-142490OB-C32 and PCI2023-146000-2, funded by MICIU/AEI/10.13039/501100011033 and co-funded by FEDER, European Union, as well as Consejeria de Educación (JCyL) through grants VA026G24 and CLU-2023-1-05. This research utilizes spectra acquired with the NASA RELAB facility at Brown University. Many thanks to Benjamin Rondeau from the Département Sciences de la Terre et de l'Univers at Nantes Université for the ruby in amphibolite sample as well as to the Collection de Minéraux at Sorbonne Université for the loan of samples. Any use of trade, firm, or product names is for descriptive purposes only and does not imply endorsement by the U.S. Government. We would like to thank Allan Treiman and an anonymous reviewer for their thoughtful reviews, which greatly improved the quality of this manuscript.

References

Anderson, R. B., Forni, O., Cousin, A., Wiens, R. C., Clegg, S. M., Frydenvang, J., et al. (2022). Post-landing major element quantification using SuperCam laser induced breakdown spectroscopy. *Spectrochimica Acta Part B-Atomic Spectroscopy*, *188*, 106347. https://doi.org/10.1016/j.sab.2021.106347

Baldwin, L. C., Tomaschek, F., Ballhaus, C., Gerdes, A., Fonseca, R. O. C., Wirth, R., et al. (2017). Petrogenesis of alkaline basalt-hosted sapphire megacrysts. Petrological and geochemical investigations of in situ sapphire occurrences from the siebengebirge Volcanic Field, Germany. *Contributions to Mineralogy and Petrology*, *172*(6), 43. https://doi.org/10.1007/s00410-017-1362-0

Beck, P., Beyssac, O., Dehouck, E., Bernard, S., Pineau, M., Mandon, L., et al. (2025). From hydrated silica to quartz: Potential hydrothermal precipitates found in Jezero crater, Mars. *Earth and Planetary Science Letters*, *656*, 119256. https://doi.org/10.1016/j.epsl.2025.119256

Bedford, C. C., Wiens, R. C., Quantin-Nataf, C., Horgan, B. H. N., Udry, A., Motta, G., et al. (2026). Impact-related alteration of the Jezero crater rim; melt formation and evidence for impact-induced hydrothermalism. *Lunar and Planetary Science Conference*.

Bell, J. F., Maki, J. N., Mehall, G. L., Ravine, M. A., Caplinger, M. A., Bailey, Z. J., et al. (2021). The Mars 2020 rover Mast Camera zoom (Mastcam-Z) multispectral, stereoscopic Imaging investigation. *Space Science Reviews*, *217*(1), 24. https://doi.org/10.1007/s11214-020-00755-x

Belley, P. M., Onodenalore, O., Abdale, L., Groat, L. A., & Fayek, M. (2025). Chemical discrimination of magmatic vs. metamorphic blue corundum: The problem of corundum formed in partial melt and its implications for sapphire exploration and deposit modeling. *Lithos*, *510*, 108125. https://doi.org/10.1016/j.lithos.2025.108125

Bersani, D., Aliatis, I., Tribaudino, M., Mantovani, L., Benisek, A., Carpenter, M. A., et al. (2018). Plagioclase composition by Raman spectroscopy. *Journal of Raman Spectroscopy*, *49*(4), 684–698. https://doi.org/10.1002/jrs.5340

Beyssac, O., Clavé, E., Forni, O., Udry, A., Pascuzzo, A. C., Dehouck, E., et al. (2026). Ultramafic float rocks at Jezero crater (Mars): Excavation of lower crustal rocks or mantle peridotites by impact cratering? *Earth and Planetary Science Letters*, *675*, 119746. https://doi.org/10.1016/j.epsl.2025.119746

Beyssac, O., Forni, O., Cousin, A., Udry, A., Kah, L. C., Mandon, L., et al. (2023). Petrological traverse of the olivine cumulate Seitah Formation at jezero crater, Mars: A perspective from SuperCam onboard perseverance. *Journal of Geophysical Research-Planets*, *128*(7), e2022JE007638. https://doi.org/10.1029/2022JE007638

Bischoff, A., & Stoffler, D. (1992). Shock metamorphism as a fundamental process in the evolution of planetary bodies - Information from meteorites. *European Journal of Mineralogy*, *4*(4), 707–755. https://doi.org/10.1127/ejm/4/4/0707

Clavé, E., Benzerara, K., Meslin, P. Y., Forni, O., Royer, C., Mandon, L., et al. (2023). Carbonate detection with SuperCam in igneous rocks on the floor of jezero crater, Mars. *Journal of Geophysical Research-Planets*, *128*(6), e2022JE007463. https://doi.org/10.1029/2022JE007463

Cousin, A., Sautter, Fabre, C., Dromart, G., Montagnac, G., Drouet, C., et al. (2022). SuperCam calibration targets on board the perseverance rover: Fabrication and quantitative characterization. *Spectrochimica Acta Part B-Atomic Spectroscopy*, *188*, 106341. https://doi.org/10.1016/j.sab.2021.106341

Dubinsky, E. V., Stone-Sundberg, J., & Emmett, J. L. (2020). A quantitative description of the causes of color in Corundum. *Gems and Gemology*, *56*(1), 2–28. https://doi.org/10.5741/gems.56.1.2

Farley, K. A., Williford, K. H., Stack, K. M., Bhartia, R., Chen, A., de la Torre, M., et al. (2020). Mars 2020 Mission Overview. *Space Science Reviews*, *216*(8), 142. https://doi.org/10.1007/s11214-020-00762-y

Fau, A., Beyssac, O., Gauthier, M., Panczer, G., Gasnault, O., Meslin, P. Y., et al. (2022). Time-resolved Raman and luminescence spectroscopy of synthetic REE-doped hydroxylapatites and natural apatites. *American Mineralogist*, *107*(7), 1341–1352. https://doi.org/10.2138/am-2022-8006

Feenstra, A., & Wunder, B. (2002). Dehydration of diasporite to corundite in nature and experiment. *Geology*, *30*(2), 119–122. https://doi.org/10.1130/0091-7613(2002)030<0119:DODTCI>2.0.Co;2

Filina, M. I., Sorokina, E. S., Botcharnikov, R., Karampelas, S., Rassomakhin, M. A., Kononkova, N. N., et al. (2019). Corundum anorthosites-kyshtymites from the south urals, Russia: A combined mineralogical, geochemical, and U-Pb Zircon Geochronological Study. *Minerals*, *9*(4), 234. https://doi.org/10.3390/min9040234

Forman, R. A., Block, S., Barnett, J. D., & Piermarini, G. J. (1972). Pressure measurement made by utilization of ruby sharp-line luminescence. *Science*, *176*(4032), 284–285. https://doi.org/10.1126/science.176.4032.284

Forni, O., Maurice, S., Gasnault, O., Wiens, R. C., Cousin, A., Clegg, S. M., et al. (2013). Independent component analysis classification of laser induced breakdown spectroscopy spectra. *Spectrochimica Acta Part B-Atomic Spectroscopy*, *86*, 31–41. https://doi.org/10.1016/j.sab.2013.05.003

Gaft, M., Reisfeld, R., & Panczer, G. (2005). *Modern luminescence spectroscopy of minerals and materials/Michael Gaft, Renata Reisfeld, Gérard Panczer*. Springer.

Gaft, M., Reisfeld, R., & Panczer, G. (2015). *Modern luminescence spectroscopy of minerals and materials*. Springer.

Galili, N., Kaplan-Ashiri, I., & Halevy, I. (2023). Cathodoluminescence of iron oxides and oxyhydroxides. *American Mineralogist*, *108*(8), 1436–1448. https://doi.org/10.2138/am-2022-8843

Garczynski, B. J., Horgan, B. H. N., Johnson, J. R., Rice, M. S., Mandon, L., Chide, B., et al. (2025). Rock coatings as evidence for late surface alteration on the floor of jezero crater, Mars. *Journal of Geophysical Research-Planets*, *130*(9), e2025JE009242. https://doi.org/10.1029/2025JE009242

Giuliani, G., Groat, L. A., Fallick, A. E., Pignatelli, I., & Pardieu, V. (2020). Ruby deposits: A review and geological classification. *Minerals*, *10*(7), 597. https://doi.org/10.3390/min10070597

Giuliani, G., Pivin, M., Fallick, A. E., Ohnenstetter, D., Song, Y., & Demaiffe, D. (2015). Geochemical and oxygen isotope signatures of mantle corundum megacrysts from the Mbuji-Mayi kimberlite, Democratic Republic of Congo, and the Changle alkali basalt, China. *Comptes Rendus Geoscience*, *347*(1), 24–34. https://doi.org/10.1016/j.crte.2014.12.003

Graham, I., Sutherland, L., Zaw, K., Nechaev, V., & Khanchuk, A. (2008). Advances in our understanding of the gem corundum deposits of the West Pacific continental margins intraplate basaltic fields. *Ore Geology Reviews*, *34*(1–2), 200–215. https://doi.org/10.1016/j.oregeorev.2008.04.006

Guguschev, C., Götze, J., & Göbbels, M. (2010). Cathodoluminescence microscopy and spectroscopy of synthetic ruby crystals grown by the optical floating zone technique. *American Mineralogist*, *95*(4), 449–455. https://doi.org/10.2138/am.2010.3291

Hainshwang, T., Fritsch, E., Gaillou, E., & Shen, A. (2024). Analysing the luminescence of gems. *Elements*, *20*, 312–317.

Horton, J. W., Kunk, M. J., Belkin, H. E., Aleinikoff, J. N., Jackson, J. C., & Chou, I. M. (2009). Evolution of crystalline target rocks and impactites in the Chesapeake Bay impact structure, ICDP-USGS Eyreville B core. *Icdp-Usgs Deep Drilling Project in the Chesapeake Bay Impact Structure: Results from the Eyreville Core Holes*, *458*(14), 277–316. https://doi.org/10.1130/2009.2458

Karmakar, S., Mukherjee, S., Sanyal, S., & Sengupta, P. (2017). Origin of peraluminous minerals (corundum, spinel, and sapphirine) in a highly calcic anorthosite from the Sittampundi Layered Complex, Tamil Nadu, India. *Contributions to Mineralogy and Petrology*, *172*(8), 67. https://doi.org/10.1007/s00410-017-1383-8

Kleinmann, B. a. R. P., & Ramdohr, P. (1971). Alpha-corundum from the lunar dust. *Earth and Planetary Science Letters*, *13*(1), 19–22. https://doi.org/10.1016/0012-821x(71)90100-2

Kobayashi, T., Sekine, T., Li, X. J., & Yamashita, Y. (2004). Observation of wavelength shifts in ruby under shock compression to 36 GPa by time-resolved luminescence spectroscopy. *Physical Review B*, *69*(5), 054108. https://doi.org/10.1103/PhysRevB.69.054108

Kornprobst, J., Piboule, M., Roden, M., & Tabit, A. (1990). Corundum-Bearing Garnet clinopyroxenites at beni-bousera (Morocco) - Original plagioclase-rich gabbros recrystallized at depth within the mantle. *Journal of Petrology*, *31*(3), 717–745. https://doi.org/10.1093/petrology/31.3.717

Li, J. Y., Zhang, A. C., Sakamoto, N., Yurimoto, H., & Gu, L. X. (2020). A new occurrence of corundum in eucrite and its significance. *American Mineralogist*, *105*(11), 1656–1661. https://doi.org/10.2138/am-2020-7361

Liu, J. H., Cao, S. Y., Zhou, D. K., Li, X. W., Wu, Y., Wang, H. B., & Li, W. X. (2022). Characteristics and formation of corundum within syenite in the Yushishan rare metal deposits in the northeastern Tibetan Plateau. *American Mineralogist*, *107*(12), 2291–2306. https://doi.org/10.2138/am-2022-8223

Liu, Y., Tice, M. M., Schmidt, M. E., Treiman, A. H., Kizovski, T. V., Hurowitz, J. A., et al. (2022). An olivine cumulate outcrop on the floor of Jezero crater, Mars. *Science*, *377*(6614), 1513–1519. https://doi.org/10.1126/science.abo2756

Maki, J. N., Gruel, D., McKinney, C., Ravine, M. A., Morales, M., Lee, D., et al. (2020). The Mars 2020 engineering cameras and microphone on the perseverance rover: A next-generation imaging System for Mars exploration. *Space Science Reviews*, *216*(8), 137. https://doi.org/10.1007/s11214-020-00765-9

Maurice, S., Wiens, R. C., Bernardi, P., Caïs, P., Robinson, S., Nelson, T., et al. (2021). The SuperCam instrument suite on the Mars 2020 rover: Science objectives and mast-unit description. *Space Science Reviews*, *217*(3), 47. https://doi.org/10.1007/s11214-021-00807-w

Moroz, I., Roth, M., Boudeulle, M., & Panczer, G. (2000). Raman microspectroscopy and fluorescence of emeralds from various deposits. *Journal of Raman Spectroscopy*, *31*(6), 485–490. https://doi.org/10.1002/1097-4555(200006)31:6<485::Aid-Jrs561>3.0.Co;2-M

Nittler, L. R., Alexander, C. M. O., Gao, X., Walker, R. M., & Zinner, E. (1997). Stellar sapphires: The properties and origins of presolar Al2O3 in meteorites. *Astrophysical Journal*, *483*(1), 475–495. https://doi.org/10.1086/304234

O'Driscoll, B., & Henry, H. (2025). Transient corundum stability in high-temperature metamorphic mineral assemblages: Insights from the British Paleogene Igneous Province. *Frontiers in Earth Science*, *13*, 1576938. https://doi.org/10.3389/feart.2025.1576938

Okumura, T., Nishido, H., Ninagawa, K., & Sakamoto, T. (2006). Cathodoluminescence and thermoluminescence studies of clay minerals. *Clay Science*, *13*, 59–68.

Oliveira, B., Griffin, W. L., Gain, S. E. M., Saunders, M., Shaw, J., Toledo, V., et al. (2021). Ti in corundum traces crystal growth in a highly reduced magma. *Scientific Reports*, *11*(1), 2439. https://doi.org/10.1038/s41598-020-79739-4

Osinski, G. R., & Pierazzo, E. (2012). *Impact cratering processes and products*. Wiley-Blackwell.

Palke, A. C., Wong, J., Verdel, C., & Avila, J. N. (2018). A common origin for Thai/Cambodian rubies and blue and violet sapphires from Yogo Gulch, Montana, USA? *American Mineralogist*, *103*(3), 469–479. https://doi.org/10.2138/am-2018-6164

Piermarini, G. J., Block, S., Barnett, J. D., & Forman, R. A. (1975). Calibration of pressure-dependence of R1 ruby fluorescence line to 195 kbar. *Journal of Applied Physics*, *46*(6), 2774–2780. https://doi.org/10.1063/1.321957

Poulsen, M. D., Keulen, N., van Hinsberg, V., Kolb, J., Frei, R., Thomsen, T. B., et al. (2024). Controls on corundum Formation: Metasomatism of ultramafic rock, Nattivit, South-East Greenland. *Journal of Petrology*, *65*(11), egae110. https://doi.org/10.1093/petrology/egae110

Poulsen, M. D., Keulen, N., van Hinsberg, V. J., Kolb, J., Frei, R., & Thomsen, T. B. (2023). Geological processes defining the formation of plumasite-type corundum in the Paleoproterozoic Isertoq Terrane, South-East Greenland. *Precambrian Research*, *385*, 106940. https://doi.org/10.1016/j.precamres.2022.106940

Quantin-Nataf, C., Dehouck, E., Beck, P., Bedford, C., Mandon, L., Beyssac, O., et al. (2025). Alteration diversity observed in the inner part of jezero Crater Rim lunar and planetary science conference.

Ragan, D. D., Gustavsen, R., & Schiferl, D. (1992). Calibration of the Ruby R(1) and R(2) fluorescence shifts as a function of temperature from 0 to 600-K. *Journal of Applied Physics*, *72*(12), 5539–5544. https://doi.org/10.1063/1.351951

Raghavan, S., Imbrie, P. K., & Crossley, W. A. (2008). Spectral analysis of R-lines and vibronic sidebands in the emission spectrum of ruby using genetic algorithms. *Applied Spectroscopy*, *62*(7), 759–765. https://doi.org/10.1366/000370208784909599

Rakotondrazafy, A. F. M., Giuliani, G., Ohnenstetter, D., Fallick, A. E., Rakotosamizanany, S., Andriamamonjy, A., et al. (2008). Gem corundum deposits of Madagascar: A review. *Ore Geology Reviews*, *34*(1–2), 134–154. https://doi.org/10.1016/j.oregeorev.2007.05.001

Rodriguez-Manfredi, J. A., Juárez, M. D., Alonso, A., Apéstigue, A., Atienza, T., Banfield, D., et al. (2021). The Mars Environmental Dynamics Analyzer, MEDA. A Suite of Environmental Sensors for the Mars 2020 Mission. *Space Science Reviews*, *217*(3), 48. https://doi.org/10.1007/s11214-021-00816-9

Rogers, A. F. (1911). On corundum-syenite (uralose) from montana. *Journal of Geology*, *19*(8), 748–751. https://doi.org/10.1086/621916

Rothamel, U., Heber, J., & Grill, W. (1983). Vibronic sidebands in ruby. *Zeitschrift Fur Physik B-Condensed Matter*, *50*(4), 297–304. https://doi.org/10.1007/Bf01470041

Royer, C., Bedford, C. C., Johnson, J. R., Horgan, B. H. N., Broz, A., Forni, O., et al. (2024). Intense alteration on early Mars revealed by high-aluminum rocks at Jezero crater. *Communications Earth and Environment*, *5*(1), 671. https://doi.org/10.1038/s43247-024-01837-2

Schuster, B., Weikusat, C., Miletich, R., Trautmann, C., Neumann, R., & Fujara, F. (2010). Influence of radiation damage on ruby as a pressure gauge. *Physical Review B*, *82*(18), 184110. https://doi.org/10.1103/PhysRevB.82.184110

Simon, J. I., Hickman-Lewis, K., Cohen, B. A., Mayhew, L. E., Shuster, D. L., Debaille, V., et al. (2023). Samples collected from the floor of jezero crater with the Mars 2020 perseverance rover. *Journal of Geophysical Research-Planets*, *128*(6), e2022JE007474. https://doi.org/10.1029/2022JE007474

Simonet, C., Fritsch, E., & Lasnier, B. (2008). A classification of gem corundum deposits aimed towards gem exploration. *Ore Geology Reviews*, *34*(1–2), 127–133. https://doi.org/10.1016/j.oregeorev.2007.09.002

Stern, R. J., Tsujimori, T., Harlow, G., & Groat, L. A. (2013). Plate tectonic gemstones. *Geology*, *41*(7), 723–726. https://doi.org/10.1130/G34204.1

Syassen, K. (2008). Ruby under pressure. *High Pressure Research*, *28*(2), 75–126. https://doi.org/10.1080/08957950802235640

Thompson, D. B., Kidd, J. D., Åström, M., Scarani, A., & Smith, C. P. (2014). A comparison of R-line photoluminescence of emeralds from different origins. *Journal of Gemmology*, *34*(4), 334–343. https://doi.org/10.15506/JoG.2014.34.4.334

Udry, A., Beyssac, O., Forni, O., Clavé, E., Bedford, C., Beck, P., et al. (2025). Igneous compositions in the rim of jezero crater using SuperCam data lunar and planetary science conference.

Udry, A., Ostwald, A., Sautter, V., Cousin, A., Beyssac, O., Forni, O., et al. (2023). A Mars 2020 SuperCam perspective on the igneous Nature of the Maaz Formation at jezero Crater and link with Seitah, Mars. *Journal of Geophysical Research-Planets*, *128*(7), e2022JE007440. https://doi.org/10.1029/2022JE007440

Voudouris, P., Mavrogonatos, C., Graham, I., Giuliani, G., Tarantola, A., Melfos, V., et al. (2019). Gemstones of Greece: Geology and crystallizing environments. *Minerals*, *9*(8), 461. https://doi.org/10.3390/min9080461

Wiens, R. C., Maurice, S., Robinson, S. H., Nelson, A. E., Cais, P., Bernardi, P., et al. (2021). The SuperCam instrument suite on the NASA Mars 2020 rover: Body unit and combined System tests. *Space Science Reviews*, *217*(1), 4. https://doi.org/10.1007/s11214-020-00777-5

Wiens, R. C., Udry, A., Beyssac, O., Quantin-Nataf, C., Mangold, N., Cousin, A., et al. (2022). Compositionally and density stratified igneous terrain in Jezero crater, Mars. *Science Advances*, *8*(34), eabo3399. https://doi.org/10.1126/sciadv.abo3399

Zhang, A. C., Jiang, Q. T., Tomioka, N., Guo, Y. J., Chen, J. N., Li, Y., et al. (2021). Widespread tissintite in strongly shock-lithified lunar Regolith breccias. *Geophysical Research Letters*, *48*(5), e2020GL091554. https://doi.org/10.1029/2020GL091554